

EP4 Receptor Conformation Sensor Suited for Ligand Screening and Imaging of Extracellular Prostaglandins^S

Michael Kurz, Michaela Ulrich, Alwina Bittner, Magdalena Martina Scharf, Jingchen Shao, Imke Wallenstein, Horst Lemoine, Nina Wettschureck, Peter Kolb, and Moritz Bünemann

Institutes for Pharmacology and Clinical Pharmacy (M.K., M.U., A.B., I.W., M.B.) and Pharmaceutical Chemistry (M.M.S., P.K.), Faculty of Pharmacy, Philipps-University Marburg, Marburg, Germany; Department of Pharmacology (J.S., N.W.), Max Planck Institute for Heart and Lung Research, Bad Nauheim, Germany; Department of Laser Medicine, Heinrich Heine University, Düsseldorf, Germany (H.L.); and LWL-Laboratory (H.L.), Düsseldorf, Germany

Received November 17, 2022; accepted June 1, 2023

ABSTRACT

Prostaglandins are important lipid mediators with a wide range of functions in the human body. They act mainly via plasma membrane localized prostaglandin receptors, which belong to the G-protein coupled receptor class. Due to their localized formation and short lifetime, it is important to be able to measure the distribution and abundance of prostaglandins in time and/or space. In this study, we present a Foerster resonance energy transfer (FRET)-based conformation sensor of the human prostaglandin E receptor subtype 4 (EP4 receptor), which was capable of detecting prostaglandin E₂ (PGE₂)-induced receptor activation in the low nanomolar range with a good signal-to-noise ratio. The sensor retained the typical selectivity for PGE₂ among arachidonic acid products. Human embryonic kidney cells stably expressing the sensor did not produce detectable amounts of prostaglandins making them suitable for a coculture approach allowing us, over time, to detect prostaglandin formation in Madin-Darby canine kidney cells and primary mouse macrophages. Furthermore, the EP4 receptor sensor proved to be suited to detect experimentally generated PGE₂ gradients by means of FRET-microscopy, indicating

the potential to measure gradients of PGE₂ within tissues. In addition to FRET-based imaging of prostanoid release, the sensor allowed not only for determination of PGE₂ concentrations, but also proved to be capable of measuring ligand binding kinetics. The good signal-to-noise ratio at a commercial plate reader and the ability to directly determine ligand efficacy shows the obvious potential of this sensor interest for screening and characterization of novel ligands of the pharmacologically important human EP4 receptor.

SIGNIFICANCE STATEMENT

The authors present a biosensor based on the prostaglandin E receptor subtype 4, which is well suited to measure extracellular prostaglandin E₂ (PGE₂) concentration with high temporal and spatial resolution. It can be used for the imaging of PGE₂ levels and gradients by means of Foerster resonance energy transfer microscopy, and for determining PGE₂ release of primary cells as well as for screening purposes in a plate reader setting.

Introduction

The communication between cells is pivotal for the function of multicellular organisms. It is heavily dependent on secreted extracellular ligands such as neurotransmitters or local mediators, which are detected via receptors by recipient cells. Receptors activated by extracellular ligands induce cellular responses, which have been studied extensively by

means of imaging spatiotemporal distribution of intracellular second messengers. However, the spatiotemporal distribution of the extracellular ligands is far more difficult to study due to the lack of suitable detectors. For the first time, and only recently, technical advances have enabled the direct measurement of neurotransmitters such as norepinephrine, ATP, dopamine, endocannabinoids, acetylcholine, and serotonin (Ravotto et al., 2020; Wu et al., 2022) with high spatial resolution. Instead of neurotransmitters, we focused on prostaglandins as local mediators and developed a Foerster resonance energy transfer (FRET)-based assay suited to detect the concentration of an extracellular ligand by means of ratiometric imaging. Prostaglandins (PGs) are important lipid mediators with a variety of crucial functions and almost ubiquitous occurrence in the human body. They are formed in an enzymatic process

This work was supported by Deutsche Forschungsgemeinschaft [Grant BU1133/5-1].

H.L. is the owner of the commercial enterprise LWL-Laboratory (Düsseldorf) and performed experiments and data analysis using the RasiDec-FRET high performance plate reader and RasiNext analysis software from LWL-Laboratories. The other authors declare no competing interests.

dx.doi.org/10.1124/molpharm.122.000648.

^S This article has supplemental material available at jmol.aspetjournals.org.

ABBREVIATIONS: AA, arachidonic acid; ASS, acetyl salicylic acid; CFP, cyan fluorescent protein; CI, confidence interval; CR, concentration ratio; DHGLA, dihomog- γ -linolenic acid; DMEM, Dulbecco's modified Eagle's medium; 8-iso, 8-isoprostanes; EPA, eicosapentaenoic acid; EP4 receptor, prostaglandin E receptor subtype 4; eYFP, enhanced yellow fluorescent protein; FRET, Förster resonance energy transfer; eYFP/mTurq2, emission ratio; GPCR, G-protein coupled receptor; HEK, human embryonic kidney; Ilo, Iloprost; LPS, lipopolysaccharide; MDCK, Madin-Darby canine kidney; MF63, phenanthrene imidazole 3; mTurq2, mTurquoise fluorescent protein 2; PG, prostaglandin; PGE₂, prostaglandin E₂; ROI, regions of interest; YFP, yellow fluorescent protein.

inside the cell and can act by autocrine as well as paracrine signaling mainly via plasma membrane localized prostaglandin receptors, which belong to the G-protein coupled receptor (GPCR) class (Woodward et al., 2011). Prostaglandins are released from many different cell types and are short lived, likely leading to local unequal concentrations of PGs in tissues or organs. Currently, the state of the art method to measure prostaglandin concentrations is a discontinuous measurement for example by means of commercially available ELISA-based kits (Ma et al., 2018; Chen et al., 2019; Reis et al., 2020). A recent study using mass spectrometry showed that the abundance of prostaglandin D₂ did not correspond to the abundance of prostaglandin synthases in uterine tissue emphasizing the need for a reliable *in situ* measurement method for prostaglandin distribution in tissue (Duncan et al., 2021). In this study focusing on prostaglandin E₂ (PGE₂), we generated a sensor based on the human prostaglandin E receptor subtype 4 (EP4 receptor), which is currently the subject of extensive research including diverse EP4 receptor ligands in clinical trials (Das and Hong, 2021). Therefore, it might also be interesting to use the sensor in the classic way (i.e., for screening purposes of this important receptor). This aspect is supported by our successful measurements with the EP4 receptor sensor in a commercial plate reader, laying the groundwork for future prostanoid screening. The sensor was sensitive to PGE₂ in the nanomolar range, and the activity could be blocked with the specific antagonist L-161,982 and provides the opportunity to study on and off kinetics of receptor activation with high precision. Because PGE₂ is an important player in inflammatory processes, we set out to show the capability of the sensor by measuring the PGE₂ release of macrophages in real time in a coculture-based approach. Finally, we show that the EP4 receptor sensor can resolve PGE₂ gradients in space and time and thus may be suitable to image PGE₂ gradients in tissue.

Materials and Methods

Plasmids and Agonist

cDNA encoding human EP4 receptor (prostaglandin E4 receptor subtype 4 [PTGR4], AY429109, catalog number: #PER0400000) was obtained from the Missouri S&T cDNA Resource Center (<http://www.cdna.org>).

Cloning. All primers for vectors and fragments were designed to have a complementary overlap of at least 12 base pairs. The primers were designed using SnapGene Viewer (GSL Biotech LLC).

Generation of FRET-Based EP4 Receptor Sensor. First, we generated EP4 receptor mTurq2 by deleting amino acids of the C-terminus of EP4 after position S364 and fusing mTurquoise 2 (mTurq2). We flanked the mTurq2 with AgeI and EcoRV. For this, EP4 receptor was amplified as a vector with forward: 5'-CAAGTAAGATATCCTCGAGTC TAGAGGGCCCG and reverse: 5'-CACCATACCGGTTGAGCAGTGTGT CCGG. mTurq2 as a fragment was amplified with the following primers: forward: 5'-CTCAACCGGTATGGTGAGCAAGGGCGAG and reverse: 5'-ACTCGAGGATATCTTACTTGACAGCTCGTCCATGCC. Subsequently, we inserted an enhanced yellow fluorescent protein (eYFP) in ICL3 of EP4 receptor mTurq2, flanked with NotI and SacII, between L223 and S259. The amino acids in between were removed. We amplified EP4 receptor mTurq2 as a vector with forward: 5'-TACAAGCCGCG GAGCTTCCGCCGCATCG and reverse: 5'-CATTGCGGCCGCGAGCG AGGTGCGGCG and eYFP as a fragment with forward: 5'-GCGGCC GCAATGGTGAGCAAGGGCGAG and reverse: 5'-CTCCGCGGCTTGTA CAGCTCGTCCATGCC. We used Q5 High-Fidelity DNA polymerase and NEBuilder HiFi DNA Assembly kit (New England Biolabs, Ipswich, MA).

In this study, we used MF63 (13217), U-46619 (16450), arachidonic acid (90010), prostaglandin D₂ (12010), prostaglandin E₂ (14010), prostaglandin E₃ (14990), 8-isoprostane (8-iso) prostaglandin E₂ (14350), prostaglandin E₁ (13010), 8-iso prostaglandin E₁ (13360), 8-iso prostaglandin F_{2α} (16350), prostaglandin E₂ ethanolamide (14012), 15-keto prostaglandin E₂ (14720), L-161,982 (10011565), and Iloprost (18215) (Cayman Chemical, Ann Arbor, MI). The compounds were dissolved as stock solutions. The stock solutions were further diluted in buffer containing 0.1% bovine serum albumin (bovine serum albumin from heat shock fraction, protease free, fatty acid free, essentially globulin free, Sigma Aldrich, 9048-46-8). See Supplemental Table 1 for the concentrations and the applied solvent of the prepared stock solutions. Acetyl salicylic acid (ASS) was a kind gift from Dr. Wibke Diederich (Institute for Pharmaceutical Chemistry, University of Marburg, Germany).

Cell Culture and Transfections

Human Embryonic Kidney 293, HT22, and Madin-Darby Canine Kidney Cell Culture and Transfections. In this study, we carried out experiments with nontransfected, transiently, or stably transfected cells. Cells were cultured in Dulbecco's modified Eagle's medium (DMEM, 4.5 g l⁻¹ glucose) supplemented with 10% FBS, 2 mM L-glutamine, 100 U ml⁻¹ penicillin, and 0.1 mg ml⁻¹ streptomycin at 37°C in a humidified atmosphere with 5% CO₂. DMEM, FBS, L-glutamine, penicillin, and streptomycin were from Capricorn Scientific GmbH (Ebsdorfergrund, Germany). To investigate the FRET-based EP4 receptor sensor, a stable cell line was generated by transfecting human embryonic kidney (HEK)293 cells with 1 μg of FRET-based EP4 receptor sensor plasmid cDNA using Effectene reagent (Qiagen, Hilden, Germany) according to the manufacturer's instructions (in a dish with 6 cm Ø), and subsequently the cells were cultured under selection with G-418. G-418 sulfate was purchased from Capricorn Scientific GmbH. HEK293T were transiently transfected in a manner analogous to the procedure described for the stable transfection of HEK293 cells with the EP4 receptor sensor: cells were transfected with 1 μg of either EP4 receptor sensor, EP4 receptor-mTurq2, EP4 wild-type (WT)-receptor, or empty pcDNA3 backbone vector. Madin-Darby canine kidney (MDCK) cells were transfected with 1 μg EP4 receptor sensor using METAfectene PRO (Biontex Laboratories GmbH, München, Germany) according to the manufacturer's instructions. HT22 cells were transfected with 1 μg EP4 receptor sensor using Attractene (Qiagen) according to the manufacturer's instructions. Transfected cells were harvested on the subsequent day (except for cAMP measurements) and seeded for measurements on the following day either on sterile, poly-L-lysine-coated glass coverslips or on poly-L-lysine-coated or uncoated (cAMP measurements) microplates.

Single-Cell FRET Measurements

FRET signals of EP4 receptor sensor were recorded from selected single cells using an inverted microscope (Axiovert 100) and a previously described measurement setup (Jelinek et al., 2021). In brief, mTurq2 was excited with short light flashes of 60 milliseconds using a LED light source (pE-100; CoolLED) with excitation intensity set to 4% for 440 nm, and the emitted donor (mTurquoise2) and acceptor fluorescence (eYFP) were recorded with a high-performance CCD camera with a sampling frequency of 0.5–1 Hz (see schematic representation in Fig. 1A). At the end of each measurement, eYFP was excited using a LED light source (pE-100; CoolLED) with excitation intensity set to 10% for 500 nm, and the eYFP fluorescence was recorded (referred to as "total eYFP"). Cells were continuously superfused with either external buffer (137 mM NaCl, 5.4 mM KCl, 2 mM CaCl₂, 1 mM MgCl₂, 10 mM HEPES, and pH 7.32) or external buffer containing ligand in the respective concentration using a pressurized perfusion system (Fig. 1, B and C; Supplemental Figs. 1A, 2, and 5). The measurements were performed at room temperature. Data were collected by the VisiView software (Visitron Systems). The collected data were corrected for background fluorescence, bleed-through, and

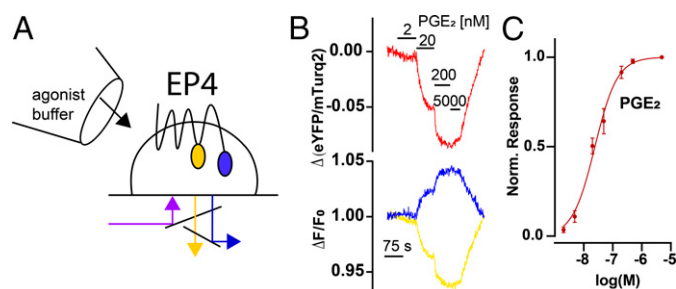


Fig. 1. EP4 receptor sensor is sensitive to PGE₂ in the low nanomolar range. (A) Scheme illustrating the principle of the FRET measurement with the EP4 receptor-based conformation sensor in single cells using a pressurized superfusion system as used for experiments shown in (B) and (C). (B) Representative traces of the emission ratio (red, baseline corrected), mTurq2 (blue), and eYFP (yellow) emission (on excitation at 440 nm, baseline-corrected and normalized to initial values) of the PGE₂-induced activation of the EP4 receptor sensor. (C) Concentration–response curve based on experiments as shown in (B) $n = 5$ each, mean \pm S.D., EC₅₀ = 24 nM (95% CI, 22–27 nM); normalized to response at 5 μ M PGE₂.

false excitation using Microsoft Excel. In detail, two regions of interest (ROI) were defined in each measurement. One ROI included the cell(s), which was/were measured, whereas the other ROI was placed at a recorded region of the coverslip, without fluorescent cells. The eYFP fluorescence of the measured cell(s) was/were subtracted by the eYFP fluorescence of the background at any given time point. The mTurq2 fluorescence was corrected in an analogous manner. In a next step, the background corrected eYFP fluorescence was subtracted by the bleed-through factor multiplied with the background-corrected mTurq2 fluorescence and by the false excitation factor multiplied with the background-corrected total eYFP fluorescence. The resulting eYFP fluorescence was then divided by the background-corrected mTurq2 fluorescence. These data were referred to as emission ratio eYFP/mTurq2. Subsequently, a correction for photobleaching (example for an uncorrected trace in Supplemental Fig. 1A) was performed by an exponential baseline subtraction using Origin 2017. These data were referred to as $\Delta(eYFP/mTurq2)$.

Determination of kinetics of receptor deactivation on agonist withdrawal was performed by fitting the corrected FRET response of EP4 receptor-sensor (see Supplemental Fig. 2) to monoexponential function, with constrained Y_0 (plateau before wash-out, which was set to 0). Only the first 30 seconds of wash-out were included for the fit. Curve-fitting and calculation of respective half-time values were performed using GraphPad Prism 8 (GraphPad Software).

FRET Measurements of Multiple Cells in the Plate Reader

For FRET measurement of multiple cells, a Spark 20M (Tecan) plate reader was used. Cells were counted and seeded in poly-L-lysine-coated Greiner Bio-One μ Clear bottom 96-well polystyrene microplates on the day before measurements. Mixtures of HEK293 and MDCK cells contained 100 000 cells each. If indicated, cells were treated with 100 μ M ASS or 5 μ M MF63 or respective vehicle solution (0.1% DMSO final) starting on the day before measurement. The respective solutions were also present during the whole course of the measurements. For experiments with HEK293 stably expressing EP4 receptor sensor alone, 120 000 cells were seeded per well. The culture medium was removed, and the cells were washed with external buffer. Subsequently, 180 μ l external buffer were placed in each well. At each application, 20 μ l external buffer or external buffer containing ligand solution were pipetted. Every protocol included the application of 20 μ l external buffer at cycle 10 except for the Z-factor value measurements, which only were pipetted once with either external buffer or external buffer containing PGE₂ at cycle 3.

Measurements were performed in the bottom reading mode using filters (bandwidth in brackets): mTurq2 was excited with 30 light

flashes at 430 nm (35) and the emitted donor fluorescence (mTurq2) and acceptor fluorescence (eYFP) were recorded at 485 nm (20) and 535 nm (25). Intensities of eYFP fluorescence was divided by that of mTurq2 fluorescence, and the resulting ratio traces were corrected for photobleaching by subtraction of a monoexponential function using Origin 2017, excluding the Z-factor value measurements. In all measurements, except for the Z-factor value measurements in each cycle, first mTurq2 was excited and the mTurq2 emission was recorded for all measured wells, followed by the excitation of mTurq2 and the recording of eYFP emission for all measured wells (measurement “whole plate mTurq2 than whole plate eYFP”). In case of the Z-factor value measurements in each cycle, every individual well was first illuminated with mTurq2, and mTurq2 was recorded and subsequently, within the same well, mTurq2 was excited and eYFP was recorded (measurement “well by well”).

Because the measurements were performed using stable cell lines, every well was considered as an individual biologic sample. Data points from at least two different days were included in every concentration–response curve.

High Resolution Multiple-Cell FRET Measurements

Based on early development work in the Institute of Lasermedicine at the Heinrich Heine University of Düsseldorf, (Lemoine and Rood, 2006; Fischer et al., 2010), novel 12-channel readers (RasiDec-FRET) were developed in the LWL-Laboratory (info@LWL-Laboratory.de), equipped with two detectors with Si photodiodes (Hamamatsu, Japan) and high precision transpedance amplifiers (integrators, Texas Instruments). A specialized injection technique with 12-channel injectors and thin stainless-steel needles (\emptyset , 1.2 mm; length, 50 mm) specially shaped to swirl the injected solutions was used to inject active substances while fluorescence measurement was in progress allowing to monitor the kinetics from the very beginning of drug action (Ilyaskina et al., 2018). The temperature of RasiDec-FRET readers was stabilized at 24°C using refrigerated circulators (Julabo F25) to perfuse the aluminum housing of RasiDec-FRET readers.

HEK293 cells stably expressing EP4 receptor sensor were seeded for 18–24 hours in black Greiner BioOne 384 well plates, 30 000 cells per well. Before starting the measurement, DMEM medium was replaced by a buffer containing (mM) 130 NaCl, 5.0 KCl, 4.8 NaHCO₃, 1.0 MgCl₂, 2.0 CaCl₂, 20 HEPES, pH 7.4, and 2% Brilliant Black at 24°C with a final volume of 120 μ l per well. Brilliant Black was purchased from Sigma-Aldrich (St. Louis, MO). Injections of test compounds (PGE₂, antagonist) were made with a volume of 10.4 μ l using the specialized injection technique described above.

For technical reasons, measurements were performed in duplicates. Thus, four runs of the 12 channels detector on wells organized in duplicates result in $n = 4$ duplicate determinations for each concentration.

RasiDec-FRET readers are controlled by a software program (RasiNext RN1012, LWL-Laboratory; info@LWL-Laboratory.de) during the measurements, which is also used for the postprocessing of data stored in a SQLITE database. Postprocessing routines were used for scaling, graphic export, the correction of the measurement curves on the basis of the control curves, calculation of mean value curves, and mean values of equilibrium effects being exported to GraphPad Prism.

Optical/Digital Equipment Used for Multiple-Cell FRET Imaging. Fluorescence was excited with violet LED-light of 435 nm (additional band-pass of 435/20 nm) for 8 milliseconds followed by darkness for 4 milliseconds, and the emitted light was split by a dichroic mirror (511 nm) and filtered by bandpass filters of 483/16 nm and 540/25 nm for the detection of blue (CFP) and yellow light (YFP), respectively. The emission of the split light was measured by a dual detector equipped with 2×12 channels for two emission wavelengths consisting of low noise silicone photodiodes (Hamamatsu Photonics, Japan) connected to so-called integrators (Texas Instruments) for the smoothing of analog data, followed by digitizing with 96 kHz analog-digital converters (Texas Instruments) and further digital smoothing

by sampling on chip before digitized data were sent (~ 100 Hz for 2×12 channels) to fast laptops (Intel i5 processors with 8 GB Ram and 256 GB SSD hard drives).

Computer software (RasiNext RN1012, LWL-Laboratory) allows us to control RasiDec-FRET readers (processing) during the experiment and provides a set of procedures for the evaluation of the data (postprocessing). RasiNext software allows a continuous recording of fluorescence, for the instantaneous display on the laptop screens, for the documentation of the injection marks, drug concentrations and any other descriptors of the experiment and for the storing of data in SQLITE data files for a subsequent data analysis.

A subroutine of the RasiNext Programm 1.2.2.8 was programmed to fit exponential curves according to a single-term

$$F(t) = F_0 \cdot [1 - \exp(-kapp \cdot t)] \quad (1)$$

and a two-term exponential model

$$F(t) = F_0 \cdot [1 - f_1 \cdot \exp(-kapp_1 \cdot t) - (1 - f_1) \cdot \exp(-kapp_2 \cdot t)] \quad (2)$$

where $F(t)$ and F_0 represent the fluorescence at time t and $t = 0$ second, respectively, $kapp$ represents the apparent association constants for the single-term model, and $kapp_1$ and $kapp_2$ represent the time constants for two classes of receptor states, a fast and a slow one, with the fractional occurrence of f_1 , and $(1 - f_1)$, respectively.

Nonlinear regression analyses were performed with R nls {stats} 3.6.2 integrated via an application programming interface in RasiNext Software package 1.2.2.8 using a Gauss-Newton algorithm. Parameter estimates are given as means \pm S.E. (standard error) for the fit of individual curves (see Supplemental Table 3). Means of parameter estimates are given \pm S.D. (see Supplemental Table 4). Residual standard errors varied between 0.7 and 3.8 on up to 45 000 degrees of freedom.

Experimental Design. HEK 293 cells were cultivated in black 384-well plates with a density of 20000 cells per well for 24 hours to be assayed in the novel 12-channel readers (RasiDec-FRET) yielding full kinetics with high resolution. Experiments were performed at 37°C . Effects of PGE_2 were measured until equilibrium was reached using equilibrium effects to calculate concentration-response curves. PGE_2 was concentrated up to $100 \mu\text{M}$ allowing the investigation of a wide concentration range of PGE_2 .

The concentration ratio (CR) log was calculated as the difference of the pEC_{50} -values of the control curve and the curve in the presence of the antagonist B indexed with o and Bi , respectively.

$$\log(\text{CR}) = \text{pEC}_{50,o} - \text{pEC}_{50,Bi} \quad (3)$$

The Gaussian standard error of $\log(\text{CR})$, SD_{CR} , was calculated according to the law of error propagation using the asymptotic standard error of the nonlinear regression analysis of the respective PGE_2 concentration-response curve as follows

$$\text{SD}_{\text{CR}} = \left\{ (\text{SD}_o)^2 + (\text{SD}_{Bi})^2 \right\}^{1/2} \quad (4)$$

From eq. 3, the Schild-plot equation can easily be calculated as

$$\log(\text{CR} - 1) = m \log([B]) + \text{pK}_B \quad (5)$$

where the slope m close to 1 indicates a competitive mode of antagonism between agonist and antagonist B.

To take into account the dependence of the error size on the concentration ratio $\log(\text{CR}-1)$, weighting factors were defined as

$$\text{SD}_{\text{CR}-1} = (\text{CR}) / (\text{CR} - 1) \cdot \text{SD}_{\text{CR}} \quad (6)$$

that was included in the regression analysis of the Schild equation (Lemoine, 1992).

Cisbio cAMP Accumulation Assay

Downstream signaling was determined using the homogeneous time-resolved fluorescence cAMP Gs dynamic assay (Cisbio Bioassays,

France), measuring cAMP accumulation. HEK293T cells were transfected with the respective receptor (EP4 WT-receptor, EP4 receptor – mTurq2, EP4 receptor sensor) or empty plasmid using effectene 2 days before measurement. To check for PGE_2 production by the cells, one dish of EP4 WT-receptor transfected cells was treated with $100 \mu\text{M}$ ASS on the day prior to the measurement. All other dishes were treated with the equivalent amount vehicle (0.1% DMSO final) for the same period of time. For the measurement, cells were harvested and resuspended in assay buffer (10 mM HEPES, 137 mM NaCl, 5.4 mM KCl, 2 mM CaCl_2 , 1 mM MgCl_2 , and pH 7.32; supplemented with $100 \mu\text{M}$ 3-isobutyl-1-methylxanthine) at a cell concentration of 1000 cells/ μL . Then $5 \mu\text{L}$ of the cell solution were transferred to each well of a white, low-volume 384-well plate, and $5 \mu\text{L}$ of the respective dilution of PGE_2 ($2 \times$ final concentration in assay buffer) was added to the cells. The plate was then incubated for 1 hour at 37°C and 95% air, 5% CO_2 . After incubation, $5 \mu\text{L}$ of each of the detection reagents cAMP-D2 and anti-cAMP-Cryptant (prepared according to the recommendations of the manufacturer in the provided lysis buffer) was added to each well, and the plate was incubated for 1 hour at room temperature. Subsequently, the plate was read on a Tecan Spark 20M plate reader using the settings recommended by the manufacturer.

As a control, cells were incubated with assay buffer instead of PGE_2 . For the negative control, cells were incubated with assay buffer, and $5 \mu\text{L}$ of lysis buffer was added instead of the anti-cAMP-Cryptant. Each measurement was repeated four times in three technical replicates.

For analysis, the homogeneous time-resolved fluorescence ratio was calculated as described by the manufacturer. Data points were plotted and fitted using GraphPad Prism ($\log(\text{inhibitor})$ vs. response):

$$Y = \text{Bottom} + \frac{\text{Top} - \text{Bottom}}{1 + 10^{-(X - \text{LogIC50})}} \quad (7)$$

FRET Measurement of Macrophages

Macrophages were induced and treated as described in Kuroda and Yamashita (2003). In brief, peritoneal cells were harvested 3 days after intraperitoneal injection of thioglycolate into C57BL/6 mice. Isolated macrophages were subsequently cultured in RPMI (RPMI Medium 1640, Gibco, 21875-034) and treated for 18 hours with either $1 \mu\text{g/ml}$ lipopolysaccharides (LPS) from *Escherichia coli* (O111:B4, Sigma Aldrich, L4391) or vehicle solution. Stock solutions of LPS were prepared as 1 mg/ml LPS in Dulbecco's phosphate buffered saline (Gibco, 14190-094). These cells were subsequently harvested by trypsinizing and the additional use of a cell scraper. The harvested macrophages were counted, and 50 000 cells were seeded per 96-well plate together with 100 000 HEK293 cells stably expressing EP4 receptor sensor. The subsequent measurement was performed at the previously described measurement setup (Jelinek et al., 2021) using a $40\times$ objective (LD ACHROPLAN $40\times/0.60$ KORR Ph2 $\infty 0-2$) with a sample frequency of 0.5 Hz. The traces were corrected for photobleaching by an exponential baseline subtraction using Origin 2017 and normalized to the response caused by PGE_2 application. We measured macrophages from three different isolations. Each isolation contained the pooled cells of five animals.

Calculation of PGE_2 Per Macrophage

To calculate the PGE_2 mass per macrophage (Fig. 6D), we calculated in a first step the concentration $[c]$ of PGE_2 in the well. This was done by using the following term, which was derived from the standard Hill equation for receptor occupancy (Fischer et al., 2010) resulting after rearrangement in

$$- \log [c] = \frac{\log(\frac{1}{y} - 1)}{\text{Hillslope}} - \log(\text{EC}_{50}) \quad (8)$$

where y is the basal sensor response normalized to PGE_2 max, $\text{EC}_{50} = 27$ nM, and $\text{Hillslope} = 0.9$. EC_{50} and Hillslope values stem from the PGE_2 concentration response curve measured in the plate reader (Fig. 4C). The resulting PGE_2 concentration was then used to calculate the mass of PGE_2 per macrophage by the following formula: $m(\text{PGE}_2)/\text{macrophage} = c \times V \times M(\text{PGE}_2)/\text{number of macrophages}$. The molecular mass of PGE_2 is $352.5 \mu\text{g}/\mu\text{mol}$ (data sheet Cayman Chemicals, item number 14010). As volume (V), we used $200 \mu\text{L}$, which was the volume present in the well at the time point of the basal response. A total of 50 000 macrophages were present per 96-well plate.

To compare our value with the result of Kuroda and Yamashita (2003), we read off the value for basal PGE_2 concentration of LPS-treated C57BL/6 peritoneal mice macrophages from Fig. 1A based on the bar graph with a concentration of 8000 pg/ml. According to the *Materials and Methods*, the cell number was given with 5×10^5 cells/ml/well. Therefore, we calculated PGE_2 release per macrophage = $(8000 \text{ pg/ml})/(5 \times 10^5 \text{ cells/ml})$ which resulted in 16 fg/cell which equals 0.045 fmol/cell.

Measurements of Artificial PGE_2 Gradient (Fig. 7; Supplemental Fig. 6) and Comparison of the Expression of EP4 Receptor-mTurq2 and EP4 Receptor Sensor

HEK293 cells stably expressing EP4 receptor sensor were seeded on glass coverslips. Measurements were performed on the following day. Micropipettes were pulled on each measuring day by using a P-87 micropipette puller. Micropipettes were filled with $10 \mu\text{M}$ PGE_2 solution. The pipette was placed under optical control using the microscope on the bottom right part of the visible area, as shown in the respective bright-field images (Fig. 7; Supplemental Fig. 6). We applied pressure with a syringe that was combined with a three-way valve. FRET signals were recorded from selected regions of interest using an inverted microscope (Axiovert 135) and an oil-immersion objective (UPlanSApo 60x/1.35 Oil Olympus) with a sample frequency of 0.2 Hz. The CFP variant mTurq2 was excited with short light flashes of 50 milliseconds using a LED light source (pE-100; CoolLED) with excitation intensity set to 7% for 440 nm and emission of mTurq2 and eYFP were split by an optosplit (Chroma) and detected with a CCD camera (RETIGA-R1, Teledyne Photometrics) and stored with VisiView software (Visitron Systems). Data shown in Fig. 7 and Supplemental Fig. 6 were corrected for background fluorescence, bleed-through, and false excitation using Microsoft Excel. Data shown in Fig. 7 was subsequently corrected for photobleaching using Origin 2017. Data shown in Fig. 7 were normalized to the response to the pipetted PGE_2 . Traces shown in Supplemental Fig. 6 were normalized to the initial emission ratio before local application of PGE_2 .

To determine the expression of EP4 receptor-mTurq2 and EP4 receptor sensor in HEK293 cells, HEK293T cells were transiently transfected with the respective construct and seeded on glass coverslips. The CFP variant mTurq2 was excited and the fluorescence was detected at the setup described above in this section. The YFP variant eYFP was excited at 500 nm with LED light source (precis Excite-100, 500 nm, CoolLED) with an excitation intensity of the light source set to 3%. In case of bleaching experiments, the bleaching was performed by illumination of the respective cells at 500 nm with LED light source (precisExcite-100, 500 nm, CoolLED) with an excitation intensity of the light source set to 50% for 1 minute. After the bleaching procedure, mTurq2 and eYFP were again excited, and the respective emissions were recorded. The first five values for each emission were averaged. The data are shown in Supplemental Fig. 1C and Supplemental Table 2. Because the EP4 receptor sensor is a conformational sensor that shows FRET in the nonactive state, the mTurq2 fluorescence is consequently too low and therefore incorrect. To correct for this, eYFP was bleached as described above and

the change in mTurq2 emission was calculated before and after bleaching. The median change of (mTurq2 (before bleaching)/mTurq2 (after bleaching)) - 1 was +29% with a median eYFP bleaching of 89% (see Supplemental Table 2). We calculated the increase for mTurq2 with 33% in case of 100% eYFP bleaching and therefore multiplied all mTurq2 emission values of EP4 receptor sensor with the factor 1.33 to correct for initial FRET effect of the sensor. The individual corrected data are shown in Supplemental Fig. 1C.

Data Analysis and Statistics

Data represent either an average of individual recordings or individual observations. Data are presented, if possible, as mean \pm S.D. The data were analyzed with Origin Pro 2017 or GraphPad Prism 8 (GraphPad Software) or Excel 2016. Statistical analysis was performed with one-way ANOVA with subsequent Tukey's multiple comparisons test as post hoc test. Differences were considered statistically significant for $P \leq 0.05$.

Analysis of Concentration-Response Relationships

Concentration-response relationships were evaluated for PGE_2 (Fig. 1C) and for PGE_3 (Supplemental Fig. 5A) at EP4 receptor sensor in single cell measurements. Single cells were superfused with concentrations tested, which was followed by a reference concentration. The responses of the tested concentrations were evaluated relative to the response of the reference concentration. Concentration-response relationships were evaluated for PGE_1 and PGE_2 (Fig. 4C), 8-iso PGE_2 (Fig. 4D), and arachidonic acid (Fig. 4D) in multiple cell measurements in the Tecan plate reader. Multiple cells were measured in a 96-well format. The procedure was done in a manner analogous to the PGE_2 concentration response curve at the EP4 receptor sensor measured in the high-resolution Multiple-Cell FRET system in 384-well format (Fig. 2). In each measurement, one test concentration and a reference concentration of PGE_2 were applied. The responses of the tested concentration were evaluated relative to the response of the reference concentration of PGE_2 . All concentration-response curves were fitted with GraphPad Prism 8 (log(agonist) versus response - variable slope (four parameters)) with variable Hill slope and EC_{50} , whereas top and bottom were constrained, except for PGE_3 (Supplemental Fig. 5A) with no constrain for top and for arachidonic acid (Fig. 5D) with no constrain for top and Hill slope set to 1. The following eq. 9 was used for fitting:

$$Y = \text{Bottom} + \frac{\text{Top} - \text{Bottom}}{1 + 10^{-(\log(\text{EC}_{50} - X) \times \text{Hillslope})}} \quad (9)$$

Calculation of Z-Factor Values. For comparison reasons, Z-factor values were calculated as described in Schihada et al. (2018) using the term eq. 10, which is based on the formula provided by Zhang et al. (1999):

$$Z - \text{factor value} = 1 - \frac{3SD_c + 3SD_s}{\text{average } c - \text{average } s} \quad (10)$$

where S.D. and average are the S.D.s and average ΔFRET [%] values of $1 \mu\text{M}$ PGE_2 (sample, s) and external buffer control (control, c), respectively. Control wells are shown in black (buffer application) and sample wells in red (PGE_2 application).

Results

Generation of a Human EP4 Receptor-Based Sensor to Display Prostaglandin Concentration in Real Time

We constructed a human EP4 receptor conformation sensor in which mTurq2 was cloned to the truncated C-terminus and eYFP into intracellular loop three, to detect alterations in FRET on receptor activation, analog to the TP receptor sensor (Kurz et al., 2020). The subsequent characterization of

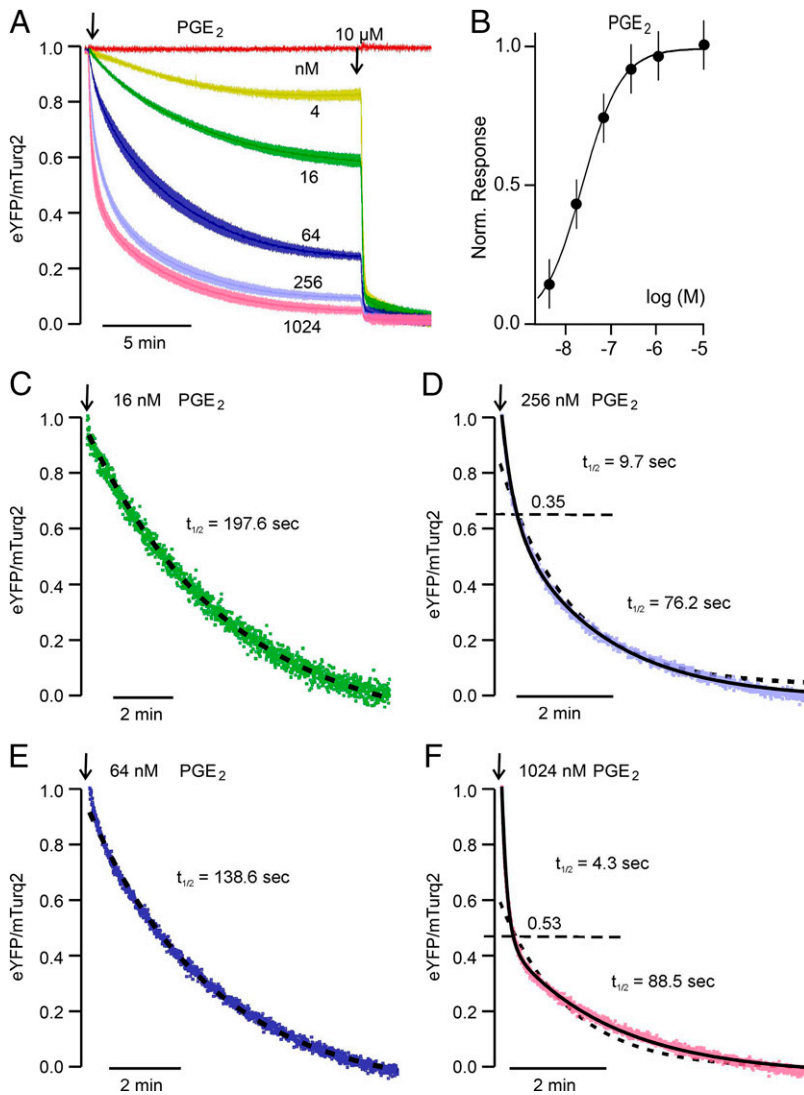


Fig. 2. Ligand binding kinetics recorded with the high resolution multiple-cell reader on EP4 receptor-sensor cells. (A) Effects of increasing concentrations of PGE₂, $n = 4$ for each condition, were normalized to maximum effects induced with 10 μ M PGE₂. A buffer injection without ligand was applied in control channels (red). Data were recorded with 41 Hz and plotted after gentle smoothing (rolling mean, $k = 4$); the shaded areas show the S.E.M. at each point. (B) Equilibrium effects were used to determine a concentration-response curve with an EC₅₀ of 21.3 ± 3.7 nM and a Hill slope of 1.01 ± 0.13 (data show mean and S.D. for $n = 4$ duplicates). (C–F) Selected curves ($N = 1$) were taken from the data set of (A) and analyzed according to a single-term (dashed line) and, for higher PGE₂ concentrations, to a two-term exponential model (eq. 3, solid line, D and F). Horizontal dashed lines at 0.35 (D) and 0.53 (F) indicate the proportion of fast components. Parameter estimates and S.E. are shown in Supplemental Table 3. Kinetic data for the entire set of curves are given as means \pm S.D. in Supplemental Table 4.

the construct was initially carried out in single-cell FRET experiments by means of dual emission fluorescence microscopy using a pressurized perfusion system (Fig. 1A). On stimulation with different concentrations of PGE₂, the emission ratio (eYFP/mTurq2) decreased in a concentration-dependent manner (Fig. 1B, top). The simultaneous eYFP-emission decrease together with an mTurq2-emission increase indicated the occurrence of FRET (Fig. 1B, bottom). The change in emission ratio was dependent on the concentration of PGE₂ and reversible on agonist withdrawal. The agonist-induced decrease in emission ratio was in line with previously published analogously constructed GPCR–FRET-conformation sensors (Kauk and Hoffmann, 2018; Kurz et al., 2020). The traces shown in Fig. 1B were corrected for photobleaching by subtraction of a monoexponential function (for the respective uncorrected trace, see Supplemental Fig. 1A). Similar baseline corrections were done for all experiments in this study if not otherwise stated. To determine the sensitivity of the sensor, we measured the dependence of the alterations in FRET by the concentration of PGE₂. The curve gave rise to an EC₅₀ value of 24 nM (95% CI, 22–27 nM) showing that this sensor allows the detection of PGE₂ in the low nanomolar range (Fig. 1C).

The observed EC₅₀ value is approximately one order of magnitude right-shifted compared with the K_i value reported in the literature to be approximately 1–2 nM for PGE₂ at the EP4 receptor (Boie et al., 1997; Kiriya et al., 1997; Abramovitz et al., 2000; Davis and Sharif, 2000; Ross et al., 2002; Araki et al., 2017). This already indicates that the sensor is likely uncoupled from G-protein signaling. We supported this assumption by measurements using a commercial kit to quantify cAMP production. The EP4 receptor sensor was, by a factor of approximately 75, less efficient to induce cAMP production compared with EP4 WT-receptors (Supplemental Fig. 1B). Interestingly, we observed basal activity for EP4 WT-receptors and EP4 receptor labeled with mTurq2, presumably due to overexpression. Furthermore, even PGE₂ application to cells, which were only transfected with empty pcDNA3 vector, caused cAMP production in a concentration-dependent manner with a right-shifted EC₅₀ by a factor of approximately 565 compared with EP4 WT-receptors (Supplemental Fig. 1B). HEK293 cells endogenously express EP4 receptor as well as other prostanoid receptors based on mRNA levels (Atwood et al., 2011), which presumably explains the response to PGE₂ of cells transfected with empty pcDNA3. The assay buffer was supplemented with

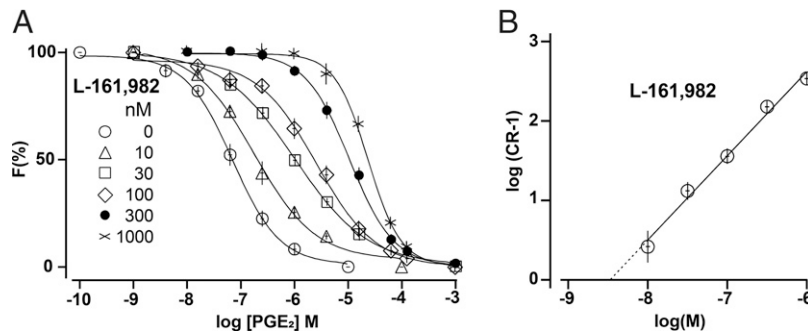


Fig. 3. Schild-plot analysis of the mode of antagonism of PGE₂ effects by L-161,982. HEK293 cells stably transfected with the PGE₂ receptor sensor were pretreated with L-161,982 at 37°C for at least 15 minutes before a concentration–effect curve for PGE₂ was started. Experiments were carried out in the new 12-channel fluorescence measuring devices (RasiNext-FRET) that facilitate the measurement of equilibrium effects (compare Fig. 2) used to determine concentration–effect curves for PGE₂ (A, data are shown as $n = 4$ duplicates, \pm S.D.). Curves were fitted by nonlinear regression, and pEC₅₀-values were used to calculate CRs for PGE₂ in the absence and presence of the antagonist. The double log plot of (CR-1)-values dependent on the concentration of L-161,982 (B) shows a linear relationship with a slope of 1.06 ± 0.04 and an abscissa intercept of 8.47 ± 0.06 ($-\log M$) characterizing L-161,982 as a competitive antagonist.

100 μ M of the phosphodiesterase inhibitor 3-isobutyl-1-methyl-xanthine, leading to cAMP accumulation and therefore further enhances the sensitivity toward the PGE₂-induced increase in cAMP levels. We compared the expression level of EP4 receptor sensor to the expression of EP4 receptor labeled with mTurq2 and observed that the EP4 receptor sensor expression was 58% of the expression level measured for EP4 receptor labeled with mTurq2 (Supplemental Fig. 1C), indicating that a reduced expression of the EP4 receptor-sensor could account only to a very minor extent for the much-reduced cAMP production of the sensor compared with the EP4 receptor mTurq2.

We next measured EP4 receptor sensor stably expressed in HEK293 cells in 384-well format plates (30 000 cells/well) using the optimized high performance multicell reader system (RasiDec-FRET, LWL-Laboratory). These measurements indicated activation kinetics of PGE₂ at the EP4 receptor, which presumably directly reflect binding kinetics (Fig. 2) nicely showing the acceleration of drug onset with increasing PGE₂ concentrations and stable equilibrium-effects. We observed that the activation kinetics of concentrations higher than approximately 100 nM PGE₂ were biphasic and could be best fitted with a two-component exponential function. The time constant of the fast phase was inversely dependent on the agonist concentration, and its fractional size was positively correlated with the agonist concentration (Fig. 2, D and F) and therefore likely reflects the actual binding-induced conformational change of the receptor. On application of 1 μ M PGE₂, the receptor activated with a half time of 4.4 second (Supplemental Table 3, two-term model) indicating a speed of activation similar in range as observed for aminergic receptors at 1 μ M agonist (Vilardaga et al., 2003; Hoffmann et al., 2005, 2012; Rochais et al., 2007). Additionally, we determined the half time of receptor deactivation on agonist withdrawal from single-cell FRET recordings using our pressurized perfusion system (Supplemental Fig. 2). The monoexponential decay of the signal was fitted and gave rise to a half time of 21 seconds (median value; mean, 28 seconds, S.D., ± 21 seconds). The median of k_{off} ($0.03325 \text{ seconds}^{-1}$) was then used together with the EC₅₀ of 24 nM from Fig. 1C to calculate k_{on} with $8.3 \times 10^7 \text{ M}^{-1} \text{ Min}^{-1}$ similar in range as described for norepinephrine on the α_{2A} -AR (Rinne et al., 2013).

Next, we tested the PGE₂-activated EP4 receptor sensor for inhibition by L-161,982. Stable EP4 receptor sensor cells were pretreated with several concentrations of L-161,982 ranging from 3 nM to 1 μ M assayed in the high resolution 12-channel readers at 37°C. The exponential decline of the ratio signals by PGE₂ resulted in equilibrium effects, which were used to calculate concentration–response curves (Fig. 3A), the appropriate pEC₅₀-values, and the concentration–ratios log (CR-1). The Schild-plot (Fig. 3B) exhibits a linear relationship of log (CR-1) on L-161,982 concentration with a slope close of unity (1.06 ± 0.04) and the abscissa intercept (pK_B) of 8.47 ± 0.08 ($-\log M$) indicating a high affinity competitive antagonism by L-161,982.

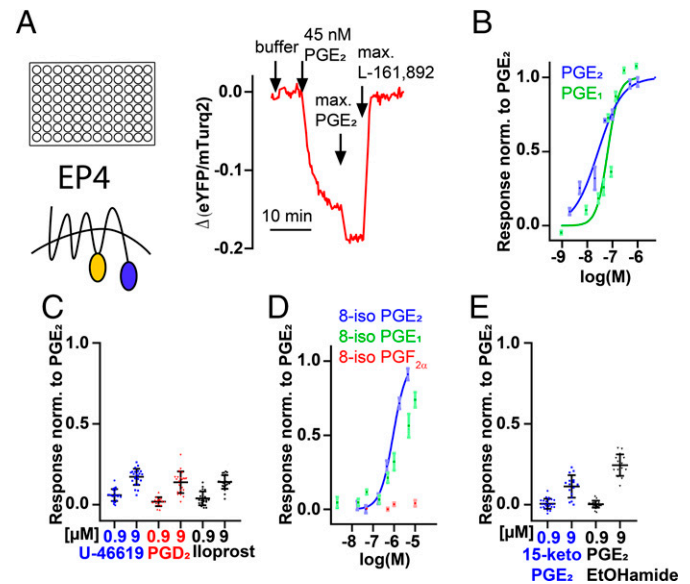


Fig. 4. EP4 receptor sensor is suited for measurements in a commercial plate reader and shows selectivity for PGE₂ among arachidonic acid products. (A) Left: scheme of FRET measurement in 96-well format at Spark 20M (Tecan) plate reader. Fluorescence of HEK293 stably expressing EP4 receptor sensor (120 k per well). Right: example trace, representative recording out of $n = 16$. (B–E) Values were normalized to the response to 833 nM PGE₂. (B) PGE₂: EC₅₀ = 27 nM (95% CI, 24–31 nM), PGE₁: EC₅₀ = 65 nM (95% CI, 58–72 nM). (D) 8-iso PGE₂ EC₅₀ = 909 nM (95% CI, 855–967 nM). (C and E) Individual values are shown. (B and D) Concentration–response curves with the indicated agonist in 96-well format. Data were plotted as mean \pm S.D. $n = 5$ –8 per data point.

Subsequently, EP4 receptor sensor signals were measured in a 96-well format (120 000 cells/well) commercially available plate reader (Fig. 4A; Supplemental Fig. 3). The transition from single cell measurements to multiple cell FRET measurements in standard plate readers is often hampered by poor signal-to-noise ratios especially for classic YFP/CFP-based GPCR conformation sensors (Schihada et al., 2018). However, using the optimized sensor of the present study resulted in an improvement of signal-to-noise ratios measurable with a commercial plate reader and enabling determination of concentration response curves for PGE₂. We calculated the Z-factor value to be 0.302 ± 0.264 (Supplemental Fig. 4, mean \pm SD), leading to the recommendation for running a double assay for screening (Zhang et al., 1999).

The EC₅₀ value of 27 nM (95% CI, 24–31 nM) PGE₂ (Fig. 4B) at the EP4 receptor sensor at the plate reader and the EC₅₀ value of 21 nM (95% CI, 16–30 nM) PGE₂ (Fig. 2B) measured on the high performance RasiDec system were comparable to the EC₅₀ value of the single-cell experiments. The EC₅₀ value of PGE₁ with 65 nM (95% CI, 58–72 nM) was also in the same range (Fig. 4B). The EC₅₀ value of PGE₃ with 67 nM (95% CI, 52–89 nM) was also similar (Supplemental Fig. 5A).

We chose the EP4 receptor as a base for our FRET sensor as this receptor possesses a high level of selectivity for PGE₂ among arachidonic acid products already at the level of the binding affinity (>factor of 500) (Boie et al., 1997; Abramovitz et al., 2000). In line with the known WT-receptor binding properties, neither a high concentration of prostaglandin D₂, Iloprost (a stable derivative of PGI₂ with higher affinity toward EP4 receptor) (Boie et al., 1997; Kiriya et al., 1997; Abramovitz et al., 2000; Davis and Sharif, 2000) nor U-46619 (a stable analog of PGH₂) were detected up to a concentration of 0.9 μ M. A concentration of 9 μ M of these compounds led to minor partial activation of the sensor (Fig. 4C). This selectivity also translated to other prostanoids such as 8-iso prostaglandins, the PGE₂ metabolite 15-keto PGE₂, and the prostamide PGE₂ ethanolamide. 8-iso PGF_{2 α} did not lead to a detectable EP4 receptor sensor activation at all, whereas 8-iso PGE₁ and PGE₂ showed a pronounced right shift of between one or two orders of magnitude compared with PGE₁ or PGE₂, respectively (Fig. 4D). Neither the PGE₂ metabolite 15-keto PGE₂ with a binding affinity of between 3 and >15 μ M at EP4 WT-receptor (Nishigaki et al., 1996; Endo et al., 2020) nor PGE₂ ethanolamide, the main COX2 product of anandamide, with an affinity comparable to that of 15-keto PGE₂ (Ross et al., 2002) were detected up to a concentration of 0.9 μ M. A concentration of 9 μ M these PGE₂ analogs led to partial activation of our sensor, despite their high degree of structural similarity in comparison with PGE₂ (Fig. 4E).

Because a recently published paper by Wu et al. (2022) on a P₂Y₁ receptor-based ATP sensor reported a difference in the affinity to ATP depending on the expression in HEK cells versus the expression in neurons of more than two orders of magnitude, we additionally tested the EP4 receptor sensor in MDCK and HT22 cells. A concentration of 30 nM PGE₂, which is close to the EC₅₀, caused a response in the same range in all three cell types indicating the robustness of our sensor independent of the applied cell type (Supplemental Fig. 5B).

Real Time Recordings of PGE₂ Release of Different Cell Types. Many different cell types produce and release prostanoids. We expressed the EP4 receptor sensor stably in HEK293 cells, which do not express detectable levels of cyclooxygenases and are therefore unable to produce prostaglandins

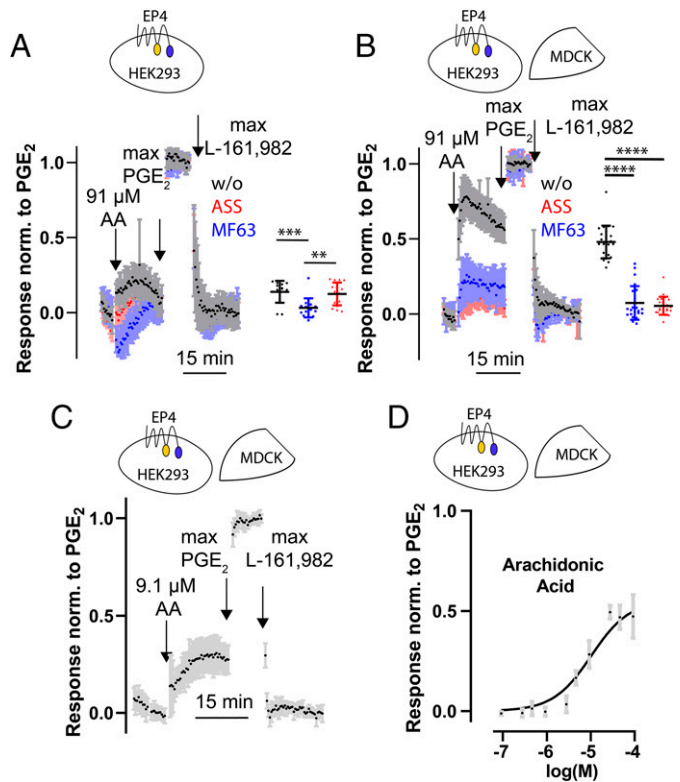


Fig. 5. Real-time measurement of prostaglandin formation in MDCK cells. HEK293 cells stably expressing EP4 receptor sensor either alone or cocultured with MDCK cells as indicated by the cartoons. The measurements were performed in 96-well format by means of a plate reader as described in Fig. 4. Cells were pretreated at least 16 hours before measurement with either 100 μ M of the COX inhibitor acetyl salicylic acid (ASS), 5 μ M of the microsomal PGE₂ synthase-1 inhibitor MF63, or the respective vehicle solution. Data are shown as mean \pm S.D. FRET alterations were normalized to the response of 833 nM PGE₂. The agonist-induced response was blocked with 3800 nM L-161,982. (A) and (B) averaged data are shown of measurements in the plate reader performed side by side; $n = 7$ –8 each, out of a total of (A) $n = 15$ –16 and (B) $n = 24$ each. Compared are the mean values before max PGE₂ application. (A) One-way ANOVA $P = 0.0002$ subsequent post hoc test: Tukey's multiple comparisons test w/o versus MF63 $***P = 0.0004$, w/o versus ASS $p = 0.8426$, and MF63 versus ASS $**P = 0.0017$. (B) One-way ANOVA $P < 0.0001$ subsequent post hoc test: Tukey's multiple comparisons test w/o versus MF63 $****P < 0.0001$, w/o versus ASS $****P < 0.0001$ and MF63 versus ASS $P = 0.7653$ (C) $n = 8$. (D) Concentration–response curve based on measurements as shown in (C) EC₅₀ = 10 μ M arachidonic acid (AA, 95% CI, 8–14 μ M).

themselves (Sood et al., 2014). Consequently, measurements of HEK293 cells stably expressing EP4 receptor sensor did not show a detectable PGE₂ production after arachidonic acid (AA) application (Fig. 5A). In contrast, MDCK cells are well known to produce and secrete detectable amounts of PGs such as PGE₂ (Levine and Ohuchi, 1978; Schaefer et al., 1996). In an experimental approach, we cocultured HEK293 cells stably expressing EP4 receptor sensor together with nontransfected MDCK cells and performed FRET measurement of multiple cells in a 96-well format. Measurement of this coculture showed PGE₂ production and release by MDCK cells. This could be specifically suppressed by either blocking the COX with acetyl salicylic acid or by using phenanthrene imidazole 3 (MF63), which has an inhibitory effect on certain prostaglandin synthases (Fig. 5B). Taken together, this experimental approach enabled the recording of PGE₂ release in real time. The resulting PGE₂ formation was related to the concentration of added arachidonic acid (Fig. 5, C and D).

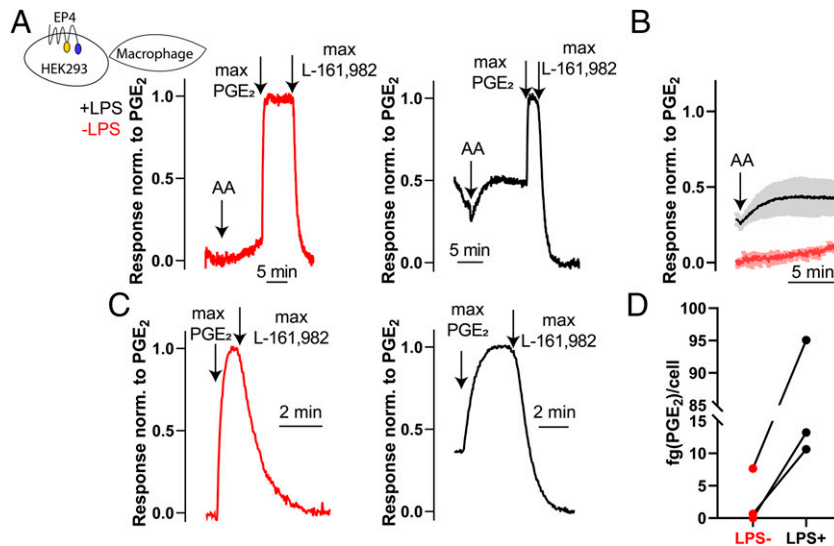


Fig. 6. Measurement of prostaglandin release of primary macrophages. HEK293 cells stably expressing EP4 receptor sensor cocultured with macrophages isolated from mice treated as described in Kuroda and Yamashita (2003) with either LPS or vehicle; the measurements were performed in 96-well format at a fluorescent microscope. We measured macrophages from three different isolations. Each isolation contained the pooled cells of five animals. If indicated, final arachidonic acid concentration was at least 27 μ M. The final concentration of PGE₂ was 833–909 nM and the final concentration of L-161,982 was 3846–4166 nM. All traces were normalized to the response to PGE₂, whereas the response to the antagonist L-161,982 was set to 0. (A) Representative traces from isolation 3. (B) Overlay of traces measured as shown in (A) from isolation 3 during the course of arachidonic acid application, data shown as mean \pm S.D.; n (LPS+) = 9, n (LPS-) = 2. (C) Representative traces of the short protocol from isolation 3 out of n = 4–6 each. (D) PGE₂ quantity was calculated based on measurements as underlying (A)–(C). For details, see *Materials and Methods* and for the exact values for each well of each isolation, see Supplemental Table 3. The wells for each isolation with and without LPS treatment were considered as a group and connected with a line.

Macrophages are well known to produce PGE₂, particularly on activation (Kuroda and Yamashita, 2003). With a similar experimental approach as used on the MDCK cells, we measured the PGE₂ release by macrophages together with HEK293 cells stably expressing EP4 receptor sensor. These measurements showed that LPS-treated macrophages caused activation of the EP4 receptor sensor that could be further enhanced by adding arachidonic acid (Fig. 6, A and B) indicating the release of PGE₂. It cannot be completely excluded that PGE₁ or PGE₃ contributed to some extent to the basal response, because the EP4 receptor (sensor) is not fully selective. We were able to quantify the PGE₂ amount present in the wells via normalization. The experimental procedure included a maximum PGE₂ response using a concentration of more than 30 times EC₅₀ followed by a subsequent saturating antagonist application (Fig. 6, A–C). Our results for two of the three isolations for the produced amount of PGE₂ per cell of LPS-treated macrophages compared well to the literature values of 16 fg/cell calculated from (Kuroda and Yamashita, 2003), who used an antibody-based assay kit versus our results: isolation 1–3 (in fg/cell \pm S.D.): 95 ± 96 , 11 ± 3 , and 14 ± 3 underlining the validity and precision of this approach (Fig. 6D).

Potential for Spatial Resolved PGE₂ Measurements. Prostanoids are often formed and act locally (Woodward et al., 2011), therefore, in many cases, their action is likely limited to the cells proximal to the prostanoid secreting cell. To see if our EP4 receptor sensor is principally capable of measuring spatial distribution of in situ-produced prostaglandins, we tested, as a first step, if the spatial distribution of an artificially generated PGE₂ gradient can be measured. To do so, we filled a patch pipette with PGE₂, placed it above HEK293 cells stably expressing the EP4 receptor sensor, and applied pressure to distribute the ligand while generating a gradient (Fig. 7, top). Cells closer

to the pipette reacted with a relatively stronger FRET change to PGE₂ than more distant cells, indicating that the sensor may be used to image the spatial distribution of PGE₂ (Fig. 7; Supplemental Fig. 6).

Discussion

In the present study, we introduce an EP4 receptor-based conformation sensor, which selectively detects PGE₂ among arachidonic acid products in the nanomolar range with high sensitivity by means of FRET. It is well suited to measure the extracellular PGE₂ concentration and has the potential to resolve PGE₂ gradients in space and time and thus might be suited to image PGE₂ gradients in tissue. Due to its high signal-to-noise ratio, the new sensor reports not only concentration-dependent activation or inhibition of the EP4 receptor but also binding and dissociation kinetics of pharmacologically active ligands as well as their efficacy akin to those described in similar receptor sensors. Therefore, this novel sensor has the potential for being used for drug screening as it works on commercially available plate readers, however, based on the Z-factor value of 0.302 ± 0.264 (Supplemental Fig. 4, mean \pm S.D.), it might not be applicable to HTS settings.

The selectivity of the EP4 receptor among arachidonic acid products for PGE₂ is very high, which is in line with the results of our experiments using our EP4 receptor sensor (Fig. 4C). The observed selectivity of our EP4 receptor sensor against PGE₂ ethanolamide (Fig. 4E) is especially striking because prostamides are often misidentified as prostaglandins by immunoassays, due to their structural similarity, which in consequence leads to the same set of antisera (Glass et al., 2005). Furthermore, it is a common feature of PGE₂ that the first

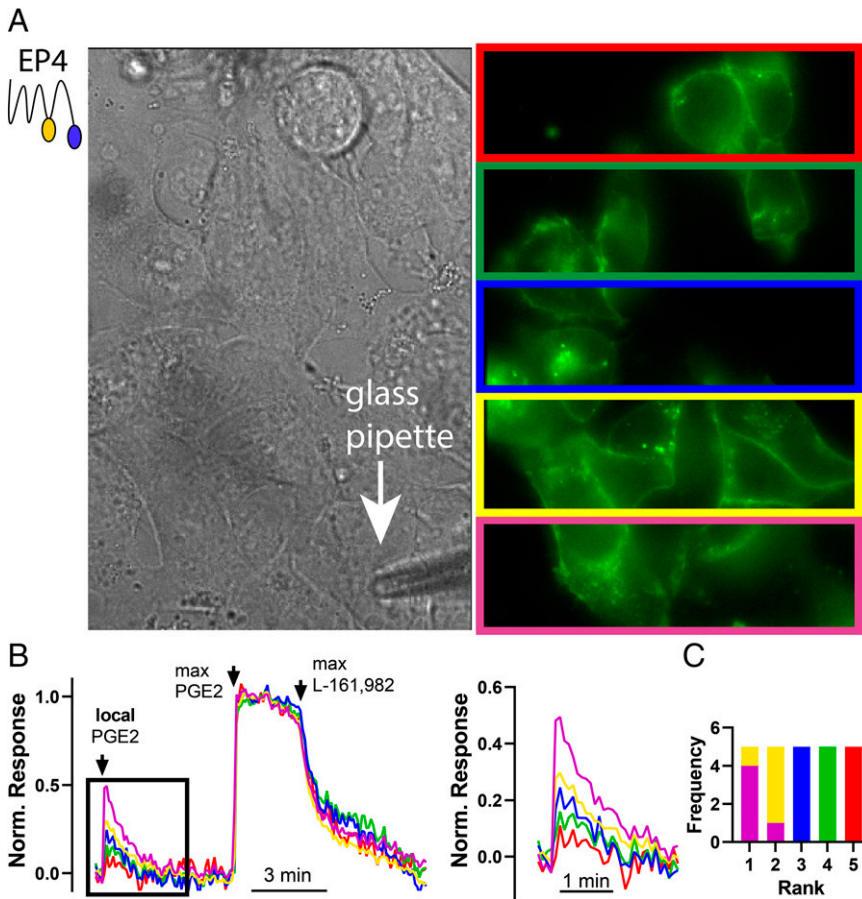


Fig. 7. EP4 receptor sensor is potentially suited for PGE₂ imaging. (A) Left: representative bright-field microscopy image of HEK293 cells stably expressing EP4 receptor sensor, glass micropipette filled with 10 μ M PGE₂. Right: respective fluorescent image, excited at 440 nM emission measured at 535 nM. (B and C) The colors refer to the outline boxes in (A). (B) Left: FRET traces from top, the colored box indicates the region of interest of the respective color. All traces were normalized to the response to max PGE₂ (final concentration: 2 μ M). Right: magnified sequence of the FRET traces shown in (B) left, marked with the black box. (C) Four more experiments were performed, similar to the experiment shown in (A) and (B) (see Supplemental Fig. 6). For comparison, the traces were normalized to the initial value before pressure application and not the maximum PGE₂ response as done in (A) and (B), for details, see *Materials and Methods*. Maximum values of each region of interest after local PGE₂ application were compared and ranked. (C) Shows the frequency distribution using the respective colors. 1 = maximum amplitude to 5 = smallest amplitude.

metabolization step eliminates much of the affinity for binding to EP4 receptors, whereas this affinity loss is much less pronounced at EP2 receptors. The selectivity factor for PGE₂ over 15-keto PGE₂ for EP2 receptor is approximately 50 in contrast to approximately 2140 for EP4 receptor, highlighting the biologic differences of PGE₂ and 15-keto PGE₂ and emphasizing the need to detect both lipids separately (Nishigaki et al., 1996; Endo et al., 2020).

It could clearly be shown (Fig. 2; Supplemental Tables 3 and 4) that small PGE₂ concentrations act monoexponentially, whereas higher PGE₂ concentrations of 256 and 1024 nM act via a bi-exponential mechanism (half times differ more than 10-fold). We hypothesize, that the short half times (single-digit seconds) represent the true association to the receptor binding pocket, whereas the slow kinetics of the small concentrations are hampered by a slow lateral diffusion in the cell membranes. The calculated k_{on} value of PGE₂ at EP4 receptor sensor with $8.31 \times 10^7 \text{ M}^{-1} \text{ Min}^{-1}$ was approximately in the range of reported antagonist k_{on} values for the DP2 receptor ranging from 4.80×10^7 to $2.23 \times 10^8 \text{ M}^{-1} \text{ Min}^{-1}$ (Sandham et al., 2017). Interestingly, the calculated k_{on} for the binding of norepinephrine (NE) to α_{2A} adrenergic receptor was only approximately a 2-fold difference (our result: k_{on} with $8.31 \times 10^7 \text{ M}^{-1} \text{ Min}^{-1}$ versus k_{on} $3.45 \times 10^7 \text{ M}^{-1} \text{ Min}^{-1}$) of Rinne et al. (2013), indicating that the completely different and far more complicated entry of PGE₂ into the binding pocket of EP4 receptors from the plasma membrane compared with the more direct entry of NE into the binding pocket of the α_{2A} -AR from the extracellular side does not make a major difference in the on-rate of binding (Rinne et al., 2013).

The Schild-plot analysis of the blockade by L-161,982 of PGE₂ revealed a competitive binding mode of L-161,982 with an affinity of approximately 3 nM. The competitive binding mode is in line with the literature whereas calculated K_i value is left shifted by approximately one order of magnitude (versus $K_i = 24 \text{ nM}$) (Machwate et al., 2001). Possible reasons for this alteration are presumably differences in experimental conditions such as incubation times or temperature, possibly leading to differences in the degree of equilibration.

In addition to the detection of the arachidonic acid product PGE₂, the EP4 receptor sensor also detects PGE₁ and PGE₃ in approximately the same concentration range (Fig. 4B; Supplemental Fig. 5A). Among prostanoids, the 2-series (arachidonic acid products) are considered most abundant (Levin et al., 2002; Wada et al., 2007). Even an artificial increase of the ratio of dihomo- γ -linolenic acid/arachidonic acid to 2.8 in LL carcinoma cells only resulted in a ratio for PGE₁/PGE₂ of 0.41, emphasizing the low abundance of PGE₁ even if dihomo- γ -linolenic acid is increased (Levin et al., 2002). Therefore, it seems reasonable to assume that a major part of the receptor sensor signal will report PGE₂ rather than PGE₁ or PGE₃.

Furthermore, there are applications in which the prostanoid series is predetermined by the experimental setting (e.g., anandamide has recently been identified as a source for arachidonic acid in the lung, likely resulting in the formation of 2-series prostaglandins rather than those of the 1-series or 3-series) (Simon et al., 2022).

Although mass spectrometry allows for the simultaneous detection of different agonists, our sensor and ELISA are limited to one ligand at a time. Furthermore, traditional ELISA showed a low specificity between series-1, -2, and -3 PGs (Kakutani et al., 2010). The sensitivity of our sensor is based on the binding properties of EP4 receptor. Based on Figs. 1B and 2A, we would assume that it shows a sensitivity range for PGE₂ of approximately 4 nM up to 200 nM. This would translate to a range of 1.4–70 ng/ml. The reported range and sensitivity of mass spectrometry and antibody-based approaches is much higher compared with our sensor, due to the high affinity of antibodies and high sensitivity of modern mass spectrometry detectors. Dependent on the concentration range of prostaglandins in tissue that may range from picomoles to nanomoles per gram of tissue (Duncan et al., 2021), the best suited method to detect overall prostaglandin concentrations should be chosen. However, in contrast to other available methods (Kakutani et al., 2010), the FRET-based detection allows for real time measurement and spatial-temporal detection of local gradients.

Our experiments with MDCK cells and macrophages (Fig. 5, B–D; Fig. 6) showed that our sensor was in the right sensitivity range to detect the prostaglandin concentrations of these types of experiments. Stimulated macrophages differ strongly in their rate of PGE₂ production. Although the C57BL mice that we used resulted in prostaglandin concentrations in the range of our sensor, experiments with BALB mice with much higher PGE₂ levels after LPS stimulation would require a less sensitive sensor (Kuroda and Yamashita, 2003). In the future, it will be important to provide sensors with lower and higher affinity to cover all crucial physiological and pathological processes involving prostaglandins, which is laborious but necessary given the biologic importance of prostanoids and specifically PGE₂.

We established a new coculture-based approach for the measurement of prostanoid formation in real time using HEK cells, which do not produce prostanoids themselves due to their lack of detectable COX. This new assay not only allowed for the measurement of prostanoid formation in cells in cell culture such as MDCK cells but also for primary cells such as the macrophages.

The activation of our EP4 receptor sensor does not involve an amplification step, enabling a quantification of the conformation change-inducing agonist. In line with this, our results for two of the three isolations for the basal produced amount of PGE₂ per LPS-treated macrophage compared well to the literature value, which involved a commercial PGE₂ immunoassay kit: 16 fg/cell versus our result isolation 1–3 (in fg/cell): 95, 11, and 14. This underlines the validity and precision of this approach (Fig. 6D; Supplemental Table 5) (Kuroda and Yamashita, 2003).

A potential drawback of using intact cells for carrying the EP4 receptor sensor could be the possibility that these cells degrade PGE₂. The similar EC₅₀ values for the PGE₂-induced EP4 receptor sensor activation obtained in single-cell assays with constant laminar superfusion of PGE₂ and in multicellular assays performed in the plate reader for which PGE₂ was pipetted in, suggest that a possible degradation of PGE₂ by HEK cells in the plate reader did not affect our results. Taken together, our coculture approach offers new research possibilities and can be applied universally to almost all type of cells, because there is no limitation by poor transfection efficiency, which makes it a valuable new tool for real time measurements of prostanoids.

Last, we could show that the EP4 receptor sensor has the potential to resolve PGE₂ gradients with spatial and temporal resolution and thus might be suited to image PGE₂ gradients in cell culture or tissue (Fig. 7).

Our FRET-based receptor sensors in comparison with recently published GPCR-based sensors (Ravotto et al., 2020; Wu et al., 2022) is a ratiometric sensor, which has the potential to quantify prostanoid concentrations independent of the expression level of our sensor.

Besides the relevance for the investigation of the prostanoid pharmacology, our new approach to measure concentrations of extracellular ligands with a FRET sensor either in coculture or in a knock-in model is of general interest. It could potentially be applied for different endogenous hormones and transmitters, such as opioids, lipid mediators, or aminergic hormones and all other types of extracellular endogenous GPCR agonists.

Acknowledgments

The authors thank M.B. Münstermann and M. Nadskakula, precision mechanics workshop of the Department of Laser Medicine, for help with the construction of the RasiDec fluorescence readers and Dr. Hannes Schihada for his help with the investigation of the EP4 receptor sensor Z-factor values.

Data Availability

The data that support the findings of this study are available on request from the corresponding author.

Authorship Contributions

Participated in research design: Kurz, Wettschureck, Kolb, Bünemann.

Conducted experiments: Kurz, Ulrich, Bittner, Scharf, Shao, Wallenstein, Lemoine.

Performed data analysis: Kurz, Ulrich, Scharf, Wallenstein, Lemoine.

Wrote or contributed to the writing of the manuscript: Kurz, Lemoine, Bünemann.

References

- Abramovitz M, Adam M, Boie Y, Carrière M, Denis D, Godbout C, Lamontagne S, Rochette C, Sawyer N, Tremblay NM et al. (2000) The utilization of recombinant prostanoid receptors to determine the affinities and selectivities of prostaglandins and related analogs. *Biochim Biophys Acta* **1483**:285–293.
- Araki Y, Suganami A, Endo S, Masuda Y, Fukushima K, Regan JW, Murayama T, Tamura Y, and Fujino H (2017) PGE1 and E3 show lower efficacies than E2 to β -catenin-mediated activity as biased ligands of EP4 prostanoid receptors. *FEBS Lett* **591**:3771–3780.
- Atwood BK, Lopez J, Wager-Miller J, Mackie K, and Straiker A (2011) Expression of G protein-coupled receptors and related proteins in HEK293, AtT20, BV2, and N18 cell lines as revealed by microarray analysis. *BMC Genomics* **12**:14.
- Boie Y, Stocco R, Sawyer N, Slipetz DM, Ungrin MD, Neuschäfer-Rube F, Püschel GP, Metters KM, and Abramovitz M (1997) Molecular cloning and characterization of the four rat prostaglandin E2 prostanoid receptor subtypes. *Eur J Pharmacol* **340**:227–241.
- Chen H, Hu B, Lv X, Zhu S, Zhen G, Wan M, Jain A, Gao B, Chai Y, Yang M et al. (2019) Prostaglandin E2 mediates sensory nerve regulation of bone homeostasis. *Nat Commun* **10**:181.
- Das D and Hong J (2021) Prostaglandin E2 receptor 4 (EP4): a promising therapeutic target for the treatment of cancer and inflammatory diseases. *Curr Chem Biol* **15**:50–68.
- Davis TL and Sharif NA (2000) Pharmacological characterization of [(3)H]-prostaglandin E(2) binding to the cloned human EP(4) prostanoid receptor. *Br J Pharmacol* **130**:1919–1926.
- Duncan KD, Sun X, Baker ES, Dey SK, and Lanekoff I (2021) In situ imaging reveals disparity between prostaglandin localization and abundance of prostaglandin synthases. *Commun Biol* **4**:966.
- Endo S, Suganami A, Fukushima K, Senoo K, Araki Y, Regan JW, Mashimo M, Tamura Y, and Fujino H (2020) 15-Keto-PGE₂ acts as a biased/partial agonist to terminate PGE₂-evoked signaling. *J Biol Chem* **295**:13338–13352.
- Fischer A, Schmidt C, Lachenicht S, Grittner D, Winkler M, Wrobel T, Rood A, Lemoine H, Frank W, and Braun M (2010) Synthesis of benzofuran, benzothiophene,

- and benzothiazole-based thioamides and their evaluation as K(ATP) channel openers. *ChemMedChem* **5**:1749–1759.
- Glass M, Hong J, Sato TA, and Mitchell MD (2005) Misidentification of prostamides as prostaglandins. *J Lipid Res* **46**:1364–1368.
- Hoffmann C, Gaietta G, Bünemann M, Adams SR, Oberdorff-Maass S, Behr B, Vilardaga J-P, Tsien RY, Ellisman MH, and Lohse MJ (2005) A FAsH-based FRET approach to determine G protein-coupled receptor activation in living cells. *Nat Methods* **2**:171–176.
- Hoffmann C, Nuber S, Zabel U, Ziegler N, Winkler C, Hein P, Berlot CH, Bünemann M, and Lohse MJ (2012) Comparison of the activation kinetics of the M3 acetylcholine receptor and a constitutively active mutant receptor in living cells. *Mol Pharmacol* **82**:236–245.
- Ilyaskina OS, Lemoine H, and Bünemann M (2018) Lifetime of muscarinic receptor-G-protein complexes determines coupling efficiency and G-protein subtype selectivity. *Proc Natl Acad Sci USA* **115**:5016–5021.
- Jelinek V, Mösslein N, and Bünemann M (2021) Structures in G proteins important for subtype selective receptor binding and subsequent activation. *Commun Biol* **4**:635.
- Kakutani S, Kawashima H, Tanaka T, Shiraishi-Tateishi A, and Kiso Y (2010) Uptake of dihomog- γ -linolenic acid by murine macrophages increases series-1 prostaglandin release following lipopolysaccharide treatment. *Prostaglandins Leukot Essent Fatty Acids* **83**:23–29.
- Kauk M and Hoffmann C (2018) Intramolecular and intermolecular FRET sensors for GPCRs – Monitoring conformational changes and beyond. *Trends Pharmacol Sci* **39**:123–135.
- Kiriyama M, Ushikubi F, Kobayashi T, Hirata M, Sugimoto Y, and Narumiya S (1997) Ligand binding specificities of the eight types and subtypes of the mouse prostanoid receptors expressed in Chinese hamster ovary cells. *Br J Pharmacol* **122**:217–224.
- Kuroda E and Yamashita U (2003) Mechanisms of enhanced macrophage-mediated prostaglandin E2 production and its suppressive role in Th1 activation in Th2-dominant BALB/c mice. *J Immunol* **170**:757–764.
- Kurz M, Krett AL, and Bünemann M (2020) Voltage dependence of prostanoid receptors. *Mol Pharmacol* **97**:267–277.
- Lemoine H (1992) β -Adrenoceptor ligands: characterization and quantification of drug effects. *Mol Inform* **11**:211–218.
- Lemoine H and Rood HA (2006) Device and method for the measurement of fluorescence in several reaction chambers. International Patent WO 2006/056168A1. 2006 Jun 1.
- Levin G, Duffin KL, Obukowicz MG, Hummert SL, Fujiwara H, Needleman P, and Raz A (2002) Differential metabolism of dihomog- γ -linolenic acid and arachidonic acid by cyclo-oxygenase-1 and cyclo-oxygenase-2: implications for cellular synthesis of prostaglandin E1 and prostaglandin E2. *Biochem J* **365**:489–496.
- Levine L and Ohuchi K (1978) Retinoids as well as tumour promoters enhance deacylation of cellular lipids and prostaglandin production in MDCK cells. *Nature* **276**:274–275.
- Ma Y, Yue Z, Zhang B, Yang M, Lao H, Lai W, Zeng Y, Chen S, and Liu P (2018) Calcium signal pathway is involved in prostaglandin E2 induced cardiac fibrosis in cardiac fibroblasts. *J Pharm Pharm Sci* **21**:326–339.
- Machwate M, Harada S, Leu CT, Seedor G, Labelle M, Gallant M, Hutchins S, Lachance N, Sawyer N, Slipetz D et al. (2001) Prostaglandin receptor EP(4) mediates the bone anabolic effects of PGE(2). *Mol Pharmacol* **60**:36–41.
- Nishigaki N, Negishi M, and Ichikawa A (1996) Two Gs-coupled prostaglandin E receptor subtypes, EP2 and EP4, differ in desensitization and sensitivity to the metabolic inactivation of the agonist. *Mol Pharmacol* **50**:1031–1037.
- Ravotto L, Duffet L, Zhou X, Weber B, Patriarchi T, and Carroll EC (2020) A bright and colorful future for G-protein coupled receptor sensors. *Front Cell Neurosci* **14**:67.
- Reis MB, Rodrigues FL, Lautherbach N, Kanashiro A, Sorgi CA, Meirelles AFG, Silva CAA, Zoccal KF, Souza COS, Ramos SG et al. (2020) Interleukin-1 receptor-induced PGE₂ production controls acetylcholine-mediated cardiac dysfunction and mortality during scorpion envenomation. *Nat Commun* **11**:5433.
- Rinne A, Birk A, and Bünemann M (2013) Voltage regulates adrenergic receptor function. *Proc Natl Acad Sci USA* **110**:1536–1541.
- Rochais F, Vilardaga JP, Nikolaev VO, Bünemann M, Lohse MJ, and Engelhardt S (2007) Real-time optical recording of β 1-adrenergic receptor activation reveals supersensitivity of the Arg389 variant to carvedilol. *J Clin Invest* **117**:229–235.
- Ross RA, Craib SJ, Stevenson LA, Pertwee RG, Henderson A, Toole J, and Ellington HC (2002) Pharmacological characterization of the anandamide cyclooxygenase metabolite: prostaglandin E2 ethanolamide. *J Pharmacol Exp Ther* **301**:900–907.
- Sandham DA, Barker L, Brown L, Brown Z, Budd D, Charlton SJ, Chatterjee D, Cox B, Dubois G, Duggan N et al. (2017) Discovery of fevipiprant (NVP-QAW039), a potent and selective DP₂ receptor antagonist for treatment of asthma. *ACS Med Chem Lett* **8**:582–586.
- Schaeffers HJ, Haselmann J, and Goppelt-Struebe M (1996) Regulation of prostaglandin synthesis in Madin Darby canine kidney cells: role of prostaglandin G/H synthase and secreted phospholipase A2. *Biochim Biophys Acta* **1300**:197–202.
- Schihada H, Vandenabeele S, Zabel U, Frank M, Lohse MJ, and Maiellaro I (2018) A universal bioluminescence resonance energy transfer sensor design enables high-sensitivity screening of GPCR activation dynamics. *Commun Biol* **1**:105.
- Simon A, von Einem T, Seidinger A, Matthey M, Bindila L, and Wenzel D (2022) The endocannabinoid anandamide is an airway relaxant in health and disease. *Nat Commun* **13**:6941.
- Sood R, Flint-Ashtamker G, Borenstein D, and Barki-Harrington L (2014) Upregulation of prostaglandin receptor EP1 expression involves its association with cyclooxygenase-2. *PLoS One* **9**:e91018.
- Vilardaga J-P, Bünemann M, Krasel C, Castro M, and Lohse MJ (2003) Measurement of the millisecond activation switch of G protein-coupled receptors in living cells. *Nat Biotechnol* **21**:807–812.
- Wada M, DeLong CJ, Hong YH, Rieke CJ, Song I, Sidhu RS, Yuan C, Warnock M, Schmaier AH, Yokoyama C et al. (2007) Enzymes and receptors of prostaglandin pathways with arachidonic acid-derived versus eicosapentaenoic acid-derived substrates and products. *J Biol Chem* **282**:22254–22266.
- Woodward DF, Jones RL, and Narumiya S (2011) International Union of Basic and Clinical Pharmacology. LXXXIII: classification of prostanoid receptors, updating 15 years of progress. *Pharmacol Rev* **63**:471–538.
- Wu Z, He K, Chen Y, Li H, Pan S, Li B, Liu T, Xi F, Deng F, Wang H et al. (2022) A sensitive GRAB sensor for detecting extracellular ATP in vitro and in vivo. *Neuron* **110**:770–782.e5.
- Zhang J-H, Chung TDY, and Oldenburg KR (1999) A simple statistical parameter for use in evaluation and validation of high throughput screening assays. *J Biomol Screen* **4**:67–73.

Address correspondence to: Moritz Bünemann, Institute for Pharmacology and Clinical Pharmacy, Faculty of Pharmacy, Philipps-University Marburg, Karl-von-Frisch-Str. 2, 35043 Marburg, Germany. E-mail: moritz.buenemann@staff.uni-marburg.de
